Check for updates

Ultralow Thermal Conductivity of Layered Bi$_2$O$_2$Se Induced by Twisting

Jie Sun, Ming Hu, Cunzhi Zhang, Ling Bai, Chenxin Zhang, and Qian Wang*

Although the twisting strategy has provided great opportunities to tune the electronic and optical properties of materials, little research has been done on how twisting affects phonon properties. Using machine-learning-based interatomic potentials within DFT-level quality and the perturbation theory to the fourth-order anharmonicity, the phonon transport properties are studied and the phonon behaviors of layered material Bi$_2$O$_2$Se when twisting is applied. It is found that the phonons of Bi$_2$O$_2$Se exhibit hardening effects at finite temperature, and the intrinsic lattice thermal conductivity along the out-of-plane (in-plane) direction is reduced to 3.21 (3.42) W/mK from 3.69 (4.55) W/mK at 300 K by including the four-phonon scattering. When introducing the twisting between the layers, the out-of-plane thermal conductivity can be further reduced by 83% as compared to that of the twist-free configuration. Such huge reduction of the thermal conductivity arises from the nearly flat acoustic phonon branches and the enhanced third- and fourth-order phonon anharmonicity due to the strong coupling between the twisted layers. These findings unravel that twisting is an effective strategy for tuning phonon band structure and phonon-phonon interactions, leading to ultralow lattice thermal conductivity of materials.

1. Introduction

Understanding phonon transport is of great interest as it plays a fundamental role in the lattice thermal conductivity (TC) of materials and thermal management applications. Materials with ultralow TC can be used for thermoelectrics, data storage devices, and thermal barrier coatings. To discover or design such materials, four key features have been proposed based on the Slack's rule,[1]: (1) Heavy atom mass, (2) weak interatomic bonding, (3) complex crystal structure, and (4) strong anharmonicity. In recent years, some other mechanisms of ultralow TC have also been suggested, such as lone pair electrons,[2] chemical bond hierarchy,[3] resonant bonding,[4] and meta-valent bonding.[5] These strategies are based on modulating chemical composition and bonding. To make a further advance, new strategies and mechanisms that can help tune the phonon transport properties to achieve ultralow TC are highly desirable.

Since Allen et al. developed the moiré bands theory in twisted bilayer graphene, the twistronics has attracted worldwide attention.[6] It has been demonstrated that by vertical stacking van der Waals materials with a small twist angle, diverse electronic and optical properties can be induced, including superconductivity,[7] correlated insulator states and orbital magnetism,[8] and topological polaritons,[9] which originate from the strong electron–electron, electron–phonon, and/or electron–photon coupling. However, much less attention has been paid to tuning the phonon–phonon interactions by twisting and understanding the underlying physical mechanism of the thermal transport properties in twisted materials. Recently, it was experimentally found that the phonon spectra of twisted bilayer MoS$_2$ can evolve rapidly over a range of small twist angles.[10] In addition, a room temperature thermal anisotropy ratio close to 900 was achieved in MoS$_2$ by random interlayer rotation, which is the highest one ever reported,[11] demonstrating that the effect of twisting on the thermal transport properties is not limited to a small angle. Currently, most of the existing studies on the twistronics have focused on 2D materials, such as bilayers, trilayers of graphene and transition metal dichalcogenide.[11,12] However, in many practical applications, the 3D structures are preferable over 2D twisted layers. In addition, experiments have shown that 3D layered GeS nanowires can be twisted, which was called the Eshelby twist, offering a new degree of freedom for tuning the optical and electrical properties.[13] Therefore, it is intuitive to wonder how the twist would affect the thermal transport properties in the 3D layered materials and what are the underlying mechanisms in determining the phonon properties under twisting.

Recently, Gibson et al.[14] experimentally measured the lattice thermal conductivities of BiOCl, Bi$_2$O$_2$Se, and Bi$_4$O$_4$SeCl$_2$ at 300 K, and found that BiOCl and Bi$_4$O$_4$SeCl$_2$ possess ultralow

J. Sun, L. Bai, C. Zhang, Q. Wang
School of Materials Science and Engineering
CAPT, BKL-MEMD
Peking University
Beijing 100871, China
E-mail: qianwang2@pku.edu.cn
M. Hu
Department of Mechanical Engineering
University of South Carolina
Columbia, SC 29208, USA
C. Zhang
Pritzker School of Molecular Engineering
University of Chicago
Chicago, IL 60637, USA

The ORCID identification number(s) for the author(s) of this article can be found under https://doi.org/10.1002/adfm.202209000.
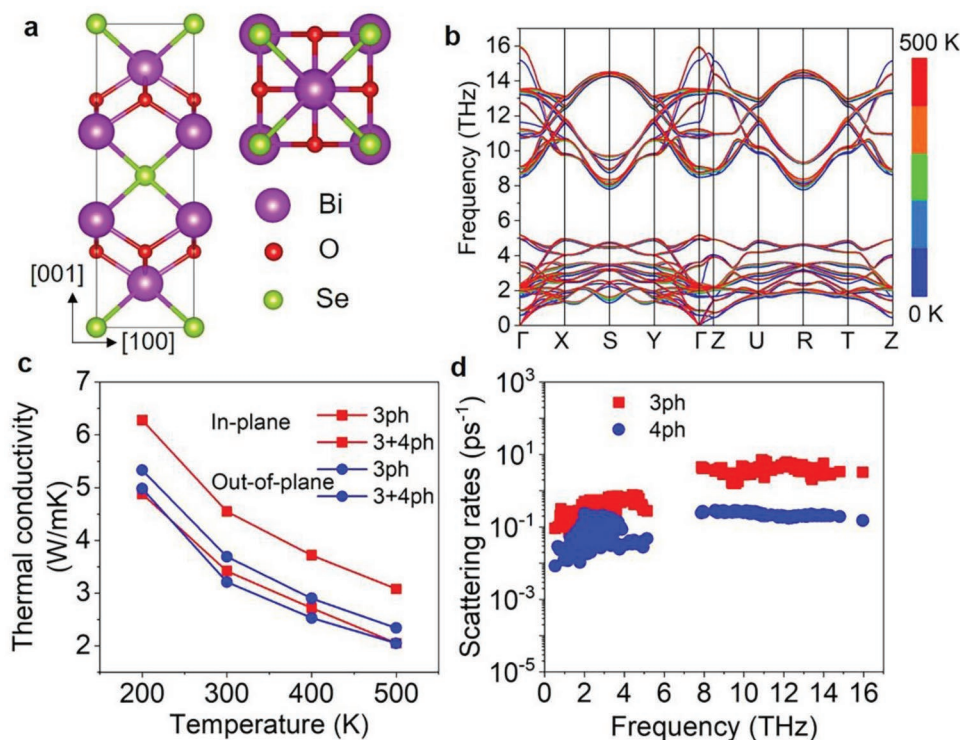
Figure 1. a) Side and top views of the optimized crystalline structure, b) temperature-dependent phonon dispersions from 0 K to 500 K, c) thermal conductivities calculated with considering three- and four-phonon scattering processes along the in-plane and out-of-plane direction, and d) three- and four-phonon scattering rates of Bi_2O_2Se.

lattice thermal conductivity of 0.15 and 0.1 W/mK along the out-of-plane direction, respectively, while the TC of Bi_2O_2Se is about ten times higher (1.0 W/mK). Because 3D Bi_2O_2Se with ultralow thermal conductivity would be a promising candidate for application in thermoelectric devices, thus the question arises: is it possible to tune the TC of Bi_2O_2Se to an ultralow value? In this letter, we demonstrate such a possibility based on a comprehensive theoretical study.

2. Results and Discussion

The optimized geometric structure of Bi_2O_2Se is shown in **Figure 1**a. One can see that the layered Bi_2O_2Se is composed of a Bi-O layer and a Se layer alternately arranged in the out-of-plane ([001] direction) with the symmetry of I4/MMM and 10 atoms in its unit cell. The optimized lattice parameters along the in-plane and out-of-plane directions are $a = b = 3.89$, and $c = 12.15$ Å, respectively, which are consistent with experimental results.[14] The detailed information of the density functional theory (DFT) calculations can be found in Supporting Information Section S1.

Based on the self-consistent phonon (SCPH) theory,[15] the temperature effect on the phonon frequency is considered. One of the key steps during the SCPH calculation is to obtain the accurate fourth force constants of crystalline structures, which demands for a large computational cost, especially the materials with lower symmetry and more atoms in their unit cells. The machine learningbased potential can effectively reduce the

computational cost. For the layered Bi_2O_2Se, the forces on each atom in a supercell are calculated using molecular dynamics (MD) simulations with moment tensor potential (MTP).[16] The detailed training settings of the MTP potential can be found in Supporting Information Section S2. After training, we find the average absolute differences for the energy and force between training and test data are 0.10 meV and 30 meV Å^{-1}, respectively. To test the accuracy of the MTP potential, we calculate the phonon dispersion of Bi_2O_2Se and compare the result with that obtained from the DFT calculation, as shown in Figure S1 (Supporting Information), which verifies the accuracy the trained MTP potential. The fourth force constants needed in the SCPH calculation are obtained from HiPhive package.[17] The details can be found in the Section 3 (Supporting Information).

We then calculate temperature-dependent phonon dispersions from 0 to 500 K of the layered Bi_2O_2Se, as shown in Figure 1b. The force constants used to obtain the temperature-dependent phonon dispersions are calculated with the machinelearning based potential. It is observed that the phonon dispersions of Bi_2O_2Se exhibit the hardening effect as temperature increases. The increased phonon frequencies in the acoustic or the optical branches can affect the phonon group velocity and the heat capacity, thus eventually influencing the thermal conductivities. Therefore, we conclude that the temperature effect on the correction of harmonic frequency is not negligible.

The thermal conductivities of the crystalline Bi_2O_2Se can be obtained by solving the linearized phonon Boltzmann transport equation (PBTE) under the single mode approximation based on the equation: $\kappa = 1/V \sum_{\lambda} c_\lambda v_\lambda^2 \tau_\lambda$, where V is the volume

**ADVANCED
SCIENCE NEWS**

www.advancedsciencenews.com

**ADVANCED
FUNCTIONAL
MATERIALS**

www.afm-journal.de

of primitive cell, c_λ, v_λ, and τ_λ are the specific heat, phonon group velocity and relaxation time, respectively, and λ is the index for the wave vector and phonon branch. Different from previous studies using the harmonic approximation to describe the phonon frequency and only considering the three-phonon interactions to obtain the phonon scattering time, which failed in the prediction of TC of many systems,[18] we use the renormalized phonon dispersions with temperature effect to calculate the phonon group velocity to obtain the TC. The calculated TC of Bi_2O_2Se including the three-phonon scattering along the out-of-plane direction at the temperature of 200, 300, 400, and 500 K is 5.33, 3.69, 2.90, and 2.34 W/mK, respectively, and the corresponding values of TC along the in-plane direction are 6.28, 4.55, 3.72, and 3.08 W/mK. One can see that the TC of the crystalline Bi_2O_2Se decreases as temperature increases, which is understandable due to the stronger phonon scattering at higher temperatures. We note that our calculated thermal conductivities are higher than the values calculated by only considering the three-phonon scattering and the vibrational frequency under the harmonic approximation in a previous study.[19] We attribute this difference to the neglect of the temperature effect in their work, which leads to the underestimation of the phonon group velocities, as evidently shown in the phonon hardening effects in Figure 1b. While, the measured thermal conductivities in experiment for Bi_2O_2Se are ≈1.0 and 1.2 W/mK along the out-of-plane and in-plane direction at room temperature, respectively,[14] which are lower than our calculated TC values when only the three-phonon interactions are considered.

Next, we include the four-phonon scattering in our calculations, as we speculate that the four-phonon scattering could have significant effect on the TC of Bi_2O_2Se. Because the unit cell of Bi_2O_2Se contains 10 atoms, the machine learning based potential and the GPU_PBTE method [20] are used to reduce the computational cost. We find that the thermal conductivities of Bi_2O_2Se along the out-of-plane and in-plane directions at the temperatures of 200, 300, 400, and 500 K are reduced to 4.98, 3.21, 2.53, and 2.05 W/mK from 5.33, 3.69, 2.90, and 2.34 W/mK, and to 4.88, 3.42, 2.72, and 2.05 W/mK from 6.28, 4.55, 3.72, and 3.08 W/mK, respectively, showing a significant reduction when the high-order scattering is included. For instance, at 300 K, the TC along the in-plane directions is reduced by 25%, namely, from 4.55 to 3.42 W/mK. The calculated three- and four-phonon scattering rates for Bi_2O_2Se are plotted in Figure 1d, which shows that the four-phonon scattering rates are comparable to the three-phonon scattering rates in the low-frequency region. Since we have used the phonon transport theory with the highest accuracy, considering the renormalized phonon frequency, three- and four-phonon scattering, the calculated thermal conductivities are still higher than those measured in the experiment. We attribute the deviation to the defects of the crystalline samples in the experiment as no real materials are without any defects. We then conduct the simulation of the diffraction to the powder pattern of the crystalline structure, and find that it is different from the results of the experimental measurement (See Supporting Information Section S4), indicating the imperfections of experimental samples.

To study the effect of twist on the TC of Bi_2O_2Se, we build three twisted structures of Bi_2O_2Se with the twist angles of 22.62°, 28.07°, and 36.87°, containing the total number of the

atoms of 260, 340, and 100 in their unit cells, respectively, based on the coincidence site lattice (CSL) theory.[21] The top views are shown in **Figure 2**a–c. We choose the twisted structure with the angle of 36.87° to calculate the phonon transport properties as it contains less atoms. We train the MTP potentials by adding the calculated forces and energy from the AIMD simulations into the original training data of the single crystal structure. The training basis and the maximum or minimum interatomic distance are the same as the settings of the single crystal structure (see Supporting Section Section S2 for the details). After training for 500 steps, the average absolute differences of the energy and force are 0.18 meV and 52 meV $Å^{-1}$, respectively.

Using the MTP potentials, we first calculate the partial phonon density of states (PDOS) of Bi_2O_2Se with and without twist, and the results are plotted in Figure 2d. We note that the phonon DOS of the Bi and O atoms in the twisted system are similar to those of the pristine structure. While some differences exist in the phonon DOS of Se atoms. The main difference is that the frequency region is broadened with red shift for some frequencies and blue shift for the others under twisting, implying that some of the bonds become stronger while some become weaker. This is understandable because the change of the structure after twisting is mainly reflected in the bonding environment around Se atoms (See Figure S3, Supporting Information). The more broaden vibrational DOS can allow more phonons existing in a small energy range, which can increase the probability of the phonon scattering. Also, the twisted system possesses a larger portion of DOS in the low frequency region, as compared with that of non-twisted one, which indicates a higher probability of the scattering among these states. The increased complexity in the bonding environment can increase the anharmonicity of the structure. The phonon dispersions of the structures with and without twist are calculated using the machinelearning based potential, as shown in Figure 2e. It is noted that the stronger coupling of different layers after twisting makes the acoustic phonon branches soften. Moreover, the transverse acoustic (TA) modes become nearly flat bands after twisting, which can cause a sharp decrease in the phonon group velocity. A similar phenomenon was found in MoS_2,[10] where the ZA branch also becomes almost flat. The flexural acoustic (ZA) modes represent the vibration along the out-of-plane direction, which is strongly suppressed by the twisting between the different layers.

It is obvious that the phonon group velocities of the twisted Bi_2O_2Se are lower than those of the pristine structure, as shown in Figure 2f. Also, in the frequency region from 0 to 1 THz, some group velocities are close to zero, which is consistent with the nearly flat bands observed in Figure 2e. This phenomenon could be a characteristic of the twisted layered material with ultralow TC.

According to the perturbation theory,[22] the three- and four-phonon scattering rates can be obtained from the third- and fourth-order interatomic force constants (IFCs), respectively:

$$\tau_{3,\lambda}^{-1} = \sum_{\lambda_1\lambda_2}\left\{\frac{1}{2}(1+n_{\lambda_1}^0+n_{\lambda_2}^0)\Gamma_- + (n_{\lambda_1}^0-n_{\lambda_2}^0)\Gamma_+\right\} \tag{1}$$

$$\tau_{4,\lambda}^{-1} = \sum_{\lambda_1\lambda_2\lambda_3}\left\{\frac{1}{6}\frac{n_{\lambda_1}^0 n_{\lambda_2}^0 n_{\lambda_3}^0}{n_\lambda^0}\Gamma_{--} + \frac{1}{2}\frac{(1+n_{\lambda_1}^0)n_{\lambda_2}^0 n_{\lambda_3}^0}{n_\lambda^0}\Gamma_{+-} + \frac{1}{2}\frac{(1+n_{\lambda_1}^0)(1+n_{\lambda_2}^0)n_{\lambda_3}^0}{n_\lambda^0}\Gamma_{++}\right\} \tag{2}$$
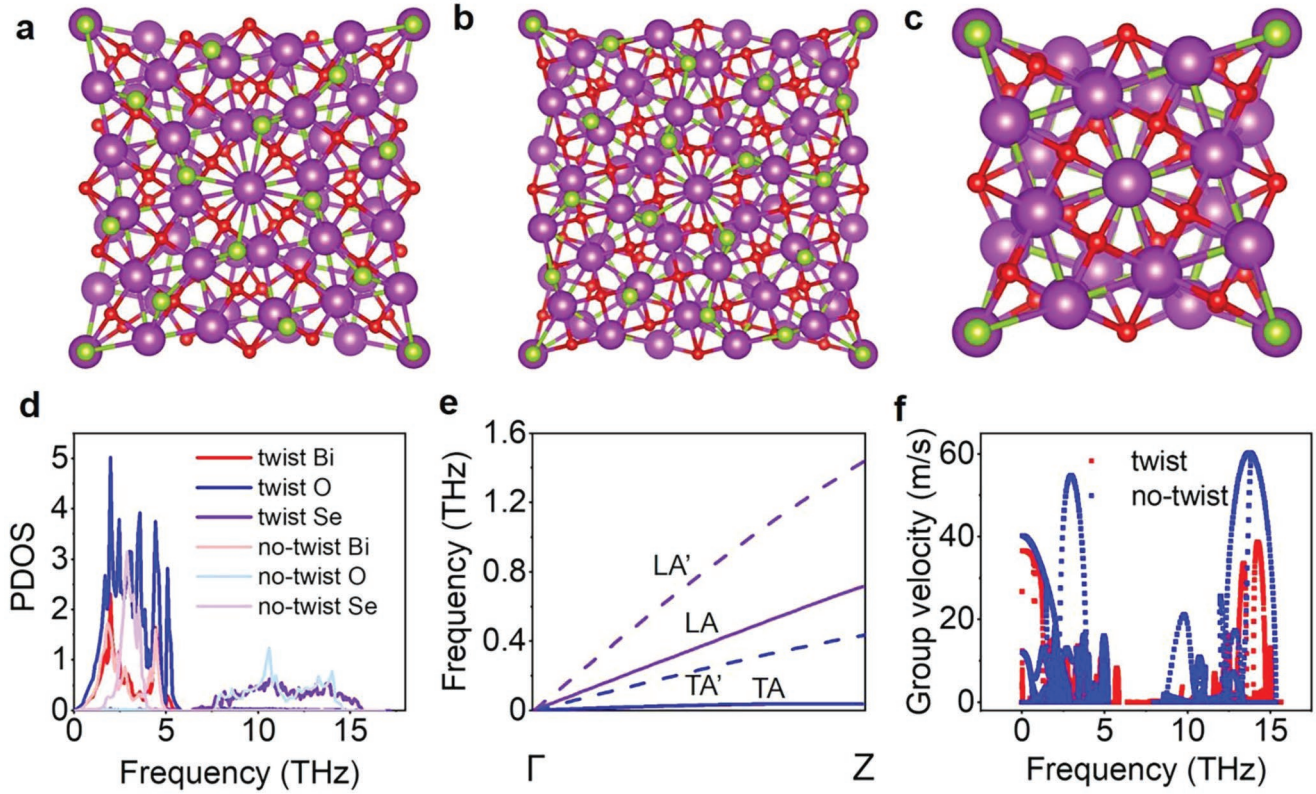
Figure 2. a–c) Top view of the geometric structure of Bi$_2$O$_2$Se with a twist angle of 22.62°,28.07°, and 36.87°, respectively. d) Partial phonon DOS, e) acoustic phonon branches of LA (LA') , TA (TA') along the path from Γ to Z, and f) phonon group velocity of Bi$_2$O$_2$Se with twist angle of 36.87° and without twist.

with

$$\Gamma_{\pm} = \frac{\pi\hbar}{4N}\left|V_{\pm}^{(3)}\right|^2 \Delta_{\pm} \frac{\delta(\omega_\lambda \pm \omega_{\lambda_1} - \omega_{\lambda_2})}{\omega_\lambda \omega_{\lambda_1} \omega_{\lambda_2}} \quad (3)$$

$$\Gamma_{\pm\pm} = \frac{\pi\hbar}{4N}\frac{\hbar}{2N}\left|V_{\pm\pm}^{(4)}\right|^2 \Delta_{\pm\pm} \frac{\delta(\omega_\lambda \pm \omega_{\lambda_1} \pm \omega_{\lambda_2} - \omega_{\lambda_3})}{\omega_\lambda \omega_{\lambda_1} \omega_{\lambda_2} \omega_{\lambda_3}} \quad (4)$$

where $V_{\pm}^{(3)}$ and $V_{\pm\pm}^{(4)}$ are

$$V_{\pm}^{(3)} = \sum_{b,l_1b_1,l_2b_2}\sum_{\alpha\alpha_1\alpha_2}\phi_{0b,l_1b_1,l_2b_2}^{\alpha\alpha_1\alpha_2}\frac{e_{ab}^\lambda e_{\alpha_1b_1}^{\pm\lambda_1}e_{\alpha_2b_2}^{-\lambda_2}}{\sqrt{\bar{m}_b\bar{m}_{b_1}\bar{m}_{b_2}}}e^{\pm ik_1\cdot\eta_1}e^{-ik_2\cdot\eta_2} \quad (5)$$

$$V_{\pm\pm}^{(4)} = \sum_{b,l_1b_1,l_2b_2,l_3b_3}\sum_{\alpha\alpha_1\alpha_2\alpha_3}\phi_{0b,l_1b_1,l_2b_2,l_3b_3}^{\alpha\alpha_1\alpha_2\alpha_3}\frac{e_{ab}^\lambda e_{\alpha_1b_1}^{\pm\lambda_1}e_{\alpha_2b_2}^{\pm\lambda_2}e_{\alpha_3b_3}^{-\lambda_3}}{\sqrt{\bar{m}_b\bar{m}_{b_1}\bar{m}_{b_2}\bar{m}_{b_3}}}e^{\pm ik_1\cdot\eta_1}e^{\pm ik_2\cdot\eta_2}e^{-ik_3\cdot\eta_3} \quad (6)$$

where $\tau_{3,\lambda}^{-1}$ and $\tau_{4,\lambda}^{-1}$ are the scattering rates including three phonons and four phonons. The primitive cell, basis atoms, and Cartesian coordinates are indexed by l, b, and α, respectively. n_λ^0 is the equilibrium occupation number. $\Gamma_\pm$ and $\Gamma_{\pm\pm}$ contains the transition probability and the transition selection rules for energy and momentum of the three and four phonons, respectively. $\phi_{0b,l_1b_1,l_2b_2}^{\alpha\alpha_1\alpha_2}$ and $\phi_{0b,l_1b_1,l_2b_2,l_3b_3}^{\alpha\alpha_1\alpha_2\alpha_3}$ are the third and fourth IFCs in the real space, respectively.

From the above equations, one can see that the scattering rates of a material are directly determined by IFCs. Therefore, we compare the differences of third-order and fourth-order

IFCs of the Bi$_2$O$_2$Se structures with and without twist based on the machinelearning potential, to study how the anharmonicity changes when the structures are under nonlinear restoring forces. **Figure 3**a,b are the illustrations of the bonding environment of the Se atom in the twisted and pristine Bi$_2$O$_2$Se structures, respectively. One can see that each Se atom is surrounded by eight Bi atoms, and when the structure is twisted, the direct change is the relative positions of the Bi atoms around the Se atom, which can have effects on the forces on the Se atom. The quartic and cubic IFCs, i.e., $\phi_{0b,l_1b_1,l_2b_2,l_3b_3}^{\alpha\alpha_1\alpha_2\alpha_3}$ and $\phi_{0b,l_1b_1,l_2b_2}^{\alpha\alpha_1\alpha_2}$, corresponding to the fourth-order and third-order derivatives of the potential energy with respect to the displacements $(\alpha\alpha_1\alpha_2\alpha_3)$ and $(\alpha\alpha_1\alpha_2)$ of quadruplets and triplets of atoms $(0b, l_1b_1,l_2b_2,l_3b_3)$ and $(0b, l_1b_1,l_2b_2)$, respectively. We choose three triplets and quadruplets, i.e., $\phi_{Se_1Se_2Bi_1}(\phi_1^{(3)})$, $\phi_{Se_1Bi_1Bi_1}(\phi_2^{(3)})$, $\phi_{Se_1Bi_2Bi_2}(\phi_3^{(3)})$ and $\phi_{Se_1Bi_1Bi_1Bi_1}(\phi_1^{(4)})$, $\phi_{Se_1Se_2Bi_1Bi_1}(\phi_2^{(4)})$, $\phi_{Se_1Se_2Se_3Bi_1}(\phi_3^{(4)})$, to make comparisons of these forces in the structure with and without twist. The IFCs of triplets and quadruplets are third-order and fourth-order tensor containing 27 and 81 force components, respectively. Figure 3c,d shows the average of the absolute value of these force components. For both triplets and quadruplets, the IFCs of the structure with twist are larger than those of the structure without twist. The difference is more obvious for the cubic IFCs, which can be explained with the Taylor series of the Born–Oppenheimer potential. We also calculate the standard deviation σ of the force components and find that the σ becomes larger for all the triplets and
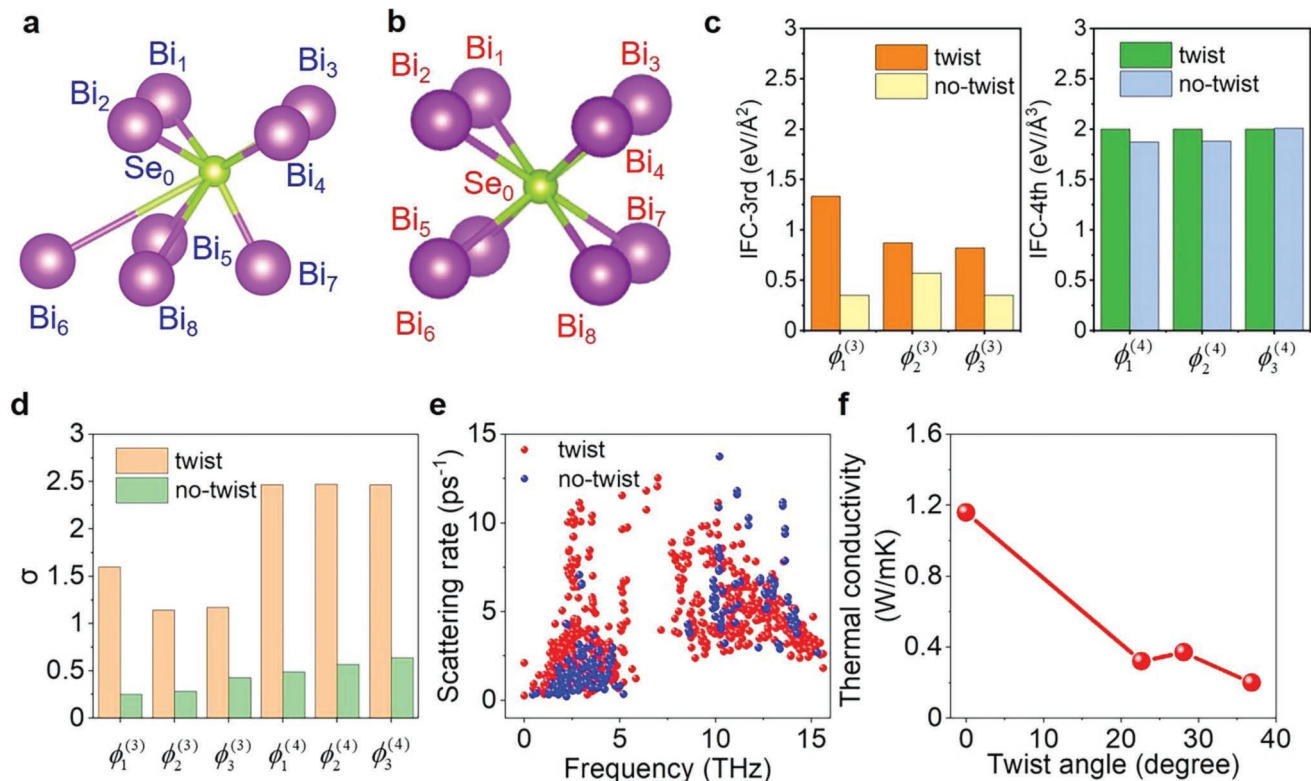
Figure 3. a, b) Bonding environment of the Se atom in the Bi_2O_2Se with twist angle of 36.87° and without twist, respectively. c) Average third and fourth force constants of the atom triplets and quadruplets in a) and b), and d) their standard deviation. e) Scattering rates of the Bi_2O_2Se with and without twist calculated using spectral energy density method. f) Change of the thermal conductivity with the twist angle of Bi_2O_2Se at 300 K obtained by using the NEMD simulations.

quadruplets after twisting, indicating the forces around the Se atom are more inhomogeneous when the structure is twisted. The larger IFCs of the triplets and quadruplets, together with a more inhomogeneous environment of the Se atom, can lead to the augmentation of $V_\pm^{(3)}$ and $V_{\pm\pm}^{(4)}$ in Equations. (5) and (6), thus enhancing the scattering rates, which is proved by the calculated scattering rates of the structures with and without twist, as shown in Figure 3e. The scattering rates are calculated via MD simulations by extracting the MD trajectories for 200 *ps* at 300 K based on the spectral energy density method (SED),[23] using the Dynaphopy package.[24] The details of this method can be found in previous work.[23a,b]

We then calculate the thermal conductivities of the twisted Bi_2O_2Se with the angle of 22.62°, 28.07°, and 36.87° and the pristine structure along the out-of-plane direction by using non-equilibrium molecular dynamics simulations (NEMD). The lengths along the out-of-plane direction of the four structures are all set as 7.2 nm to have fair comparisons. The corresponding in-plane lattice lengths of them are all set to 1.5 nm. The details can be seen in Supporting Information Section S5. The four structures are actually nanowires of Bi_2O_2Se. The calculated thermal conductivities are given in Figure 3f. As compared with the TC of 1.2 W/mK of the pristine structure, the thermal conductivities of the structures with the twist angle of 22.62°, 28.07°, and 36.87° are 0.32, 0.37, and 0.2 W/mK at 300 K, respectively. It is obvious that the TC of the twisted Bi_2O_2Se is

significantly reduced, whether the twist angle is small or large. Especially, the TC can be decreased by 83% for the structure with twist angle of 36.87°, as compared to that of the pristine Bi_2O_2Se.

It is interesting to note that thermal conductivity can also be effectively modulated in polycrystalline or amorphous materials by rotating grain boundaries,[25] where the rotation significantly changes the atomic configurations. This is different from the cases in twisted layered materials, where the in-plane atomic configurations are slightly perturbed, but the change in layer-layer coupling induced by twisting can significantly affect the phonon scattering, and flat acoustic branches can also be introduced by twisting as experimentally observed in twisted layered MoS_2.[11]

To study the size effect of the twisted structure, the length-dependent TC of the twisted Bi_2O_2Se with the angle of 36.87° is further explored. **Figure 4**a–d shows the geometric structures of the nanowires of the twisted Bi_2O_2Se with different lengths. The in-plane lattice parameters of these nanowires are all set to 1.7 nm. The calculated thermal conductivities for the different size nanowires are presented in Figure 4e. Interestingly, it is observed that the thermal conductivities reach a convergent value of 0.19 W/mK, nearly independent of the length. This can be understood from the phonon group velocity and lifetime of the Bi_2O_2Se that are sharply decreased after twisting, as shown in Figure 2f and Figure 3e. The phonons would be
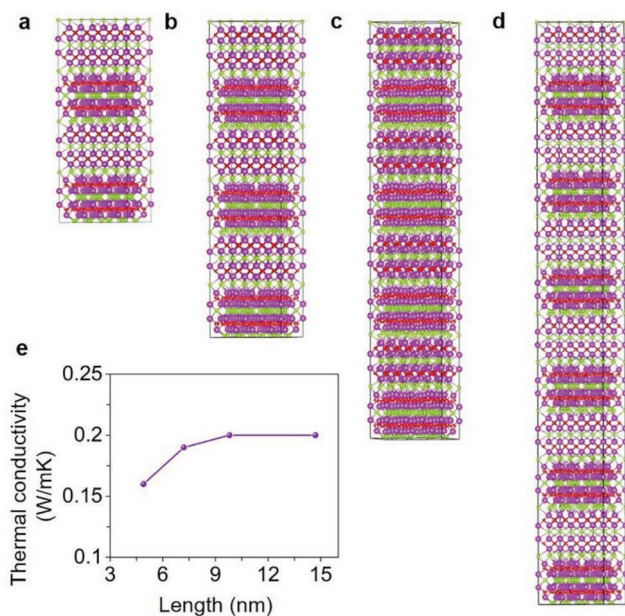
**ADVANCED
SCIENCE NEWS**
www.advancedsciencenews.com

**ADVANCED
FUNCTIONAL
MATERIALS**
www.afm-journal.de

Figure 4. a–d) Geometric structure of the twisted Bi_2O_2Se nanowire with the length of 4.9, 7.2, 9.8, and 14.6 nm, respectively. e) Change of the thermal conductivity of the twisted Bi_2O_2Se nanowire with the length.

less hindered due to the shorter phonon mean free paths, thus exhibiting an insensitive response to the size, demonstrating that the twist engineering for layered materials is an effective way to tune the TC.

Here, we only choose three twist angles of 22.62°, 28.07°, and 36.87° containing 260, 340, and 100 atoms in their unit cells, respectively, to study the change of the phonon properties with twist angle based on the machinelearning potential. In some other angles, the systems may have even lower thermal conductivities, and exhibit more interesting phenomena. However, the large unit cells containing thousands of atoms would be the problem beyond the accurate calculation from the force constants model at the current stage.

3. Conclusions

In summary, we investigate the intrinsic thermal transport properties of crystalline Bi_2O_2Se and how its thermal conductivity is modulated by twisting by using first-principles calculations combined with machine learning potential equipped NEMD simulations, which are capable of fairly treating the effects of temperature and quartic anharmonicity on the phonon energies and scattering rates. Our results show that the temperature effects on both the correction of harmonic frequency and four-phonon scattering are important in the phonon transport process, resulting in 25% decrease in the thermal conductivity at 300 K. Furthermore, we introduce the twisting in the layered material of Bi_2O_2Se, and find that the out-of-plane thermal conductivity of the twisted Bi_2O_2Se with a twist angle of 36.87° is decreased by 83% as compared to that of pristine structure, which is ascribed to the reduced phonon group velocities due

to the nearly flat acoustic (TA) phonon branches and increased anharmonicity by twisting. Our study would motivate more experimental efforts in tuning the thermal conductivity of layered materials by twisting to achieve ultralow thermal conductivity for thermoelectric applications.

Supporting Information

Supporting Information is available from the Wiley Online Library or from the author.

Conflict of Interest

The authors declare no conflict of interest.

Author Contributions

Q.W. proposed and supervised the project. J.S and M.H. carried out the research with the help of C.Z., L.B., and C.Z., and wrote the draft of the paper. All authors contributed to the revisions and discussions of the paper.

Data Availability Statement

The datasets generated and/or analyzed during the current study are available from the corresponding author upon reasonable request.

[1] G. A. Slack, *J. Phys. Chem. Solids* **1973**, *34*, 321.

[2] a) E. J. Skoug, D. T. Morelli, *Phys. Rev. Lett.* **2011**, *107*, 235901; b) G. Qin, Z. Qin, H. Wang, M. Hu, *Nano Energy* **2018**, *50*, 425.

[3] W. Qiu, L. Xi, P. Wei, X. Ke, J. Yang, W. Zhang, *Proc. Natl. Acad. Sci. USA* **2014**, *111*, 15031.

[4] S. Lee, K. Esfarjani, T. Luo, J. Zhou, Z. Tian, G. Chen, *Nat. Commun.* **2014**, *5*, 1.

[5] a) J. Y. Raty, M. Schumacher, P. Golub, V. L. Deringer, C. Gatti, M. Wuttig, *Adv. Mater.* **2019**, *31*, 1806280; b) L. Elalfy, D. Music, M. Hu, *Phys. Rev. B* **2021**, *103*, 075203; c) M. Al-Fahdi, X. Zhang, M. Hu, *J. Mater. Sci.* **2021**, *56*, 18534.

[6] R. Bistritzer, A. H. MacDonald, *Proc. Natl. Acad. Sci. USA* **2011**, *108*, 12233.

[7] a) Y. Cao, V. Fatemi, S. Fang, K. Watanabe, T. Taniguchi, E. Kaxiras, P. Jarillo-Herrero, *Nature* **2018**, *556*, 43; b) M. Yankowitz, S. Chen, H. Polshyn, Y. Zhang, K. Watanabe, T. Taniguchi, D. Graf, A. F. Young, C. R. Dean, *Science* **2019**, *363*, 1059.

[8] a) A. L. Sharpe, E. J. Fox, A. W. Barnard, J. Finney, K. Watanabe, T. Taniguchi, M. Kastner, D. Goldhaber-Gordon, *Science* **2019**, *365*, 605; b) Y. Cao, V. Fatemi, A. Demir, S. Fang, S. L. Tomarken, J. Y. Luo, J. D. Sanchez-Yamagishi, K. Watanabe, T. Taniguchi, E. Kaxiras, *Nature* **2018**, *556*, 80.

[9] G. Hu, Q. Ou, G. Si, Y. Wu, J. Wu, Z. Dai, A. Krasnok, Y. Mazor, Q. Zhang, Q. Bao, *Nature* **2020**, *582*, 209.

[10] J. Quan, L. Linhart, M.-L. Lin, D. Lee, J. Zhu, C.-Y. Wang, W.-T. Hsu, J. Choi, J. Embley, C. Young, *Nat. Mater.* **2021**, 1.

[11] S. E. Kim, F. Mujid, A. Rai, F. Eriksson, J. Suh, P. Poddar, A. Ray, C. Park, E. Fransson, Y. Zhong, *Nature* **2021**, *597*, 660.

[12] M. H. Naik, M. Jain, *Phys. Rev. Lett.* **2018**, *121*, 266401.

[13] a) Y. Liu, J. Wang, S. Kim, H. Sun, F. Yang, Z. Fang, N. Tamura, R. Zhang, X. Song, J. Wen, B. Z. Xu, M. Wang, S. Lin, Q. Yu, K. B. Tom, Y. Deng, J. Turner, E. Chan, D. Jin, R. O. Ritchie, A. M. Minor, D. C. Chrzan, M. C. Scott, J. Yao, *Nature* **2019**, *570*, 358; b) P. Sutter, S. Wimer, E. Sutter, *Nature* **2019**, *570*, 354.

[14] Q. D. Gibson, T. Zhao, L. M. Daniels, H. C. Walker, R. Daou, S. Hébert, M. Zanella, M. S. Dyer, J. B. Claridge, B. Slater, *Science* **2021**, *373*, 1017.

[15] a) N. Werthamer, *Phys. Rev. B* **1970**, *1*, 572; b) T. Tadano, S. Tsuneyuki, *Phys. Rev. B* **2015**, *92*, 054301; c) I. Errea, M. Calandra, F. Mauri, *Phys. Rev. B* **2014**, *89*, 064302.

[16] I. S. Novikov, K. Gubaev, E. V. Podryabinkin, A. V. Shapeev, *Mach Learn Sci Technol* **2020**, *2*, 025002.

[17] F. Eriksson, E. Fransson, P. Erhart, *Adv Theory Simul* **2019**, *2*, 1800184.

[18] a) Y. Xia, V. Ozoliņš, C. Wolverton, *Phys. Rev. Lett.* **2020**, *125*, 085901; b) Y. Xia, K. Pal, J. He, V. Ozoliņš, C. Wolverton, *Phys. Rev. Lett.* **2020**, *124*, 065901.

[19] R. Guo, P. Jiang, T. Tu, S. Lee, B. Sun, H. Peng, R. Yang, *Cell Rep Phys Sci* **2021**, *2*, 100624.

[20] B. Zhang, Z. Fan, C. Zhao, X. Gu, *J. Phys.: Condens. Matter* **2021**, *33*, 495901.

[21] H. Ogawa, *Mater. Trans.* **2006**, *47*, 2706.

[22] a) R. A. Cowley, *Rep. Prog. Phys.* **1968**, *31*, 123; b) T. Feng, X. Ruan, *Phys. Rev. B* **2016**, *93*, 045202.

[23] a) J. Larkin, J. Turney, A. Massicotte, C. Amon, A. McGaughey, *J. Comput. Theor. Nanosci.* **2014**, *11*, 249; b) Y. Zhou, X. Zhang, M. Hu, *Phys. Rev. B* **2015**, *92*, 195204; c) Y. Gao, X. Zhang, Y. Zhou, M. Hu, *J. Mater. Chem. C* **2017**, *5*, 10578; d) J. Sun, K. Yuan, W. Zhou, X. Zhang, J. Onoe, Y. Kawazoe, Q. Wang, *Nanotechnology* **2019**, *31*, 115701.

[24] A. Carreras, A. Togo, I. Tanaka, *Comput. Phys. Commun.* **2017**, *221*, 221.

[25] a) Y. Zhou, J.-Y. Yang, L. Cheng, M. Hu, *Phys. Rev. B* **2018**, *97*, 085304; b) Y. Zhou, X. Gong, B. Xu, M. Hu, *Nanoscale* **2017**, *9*, 9987; c) Y. Gao, Y. Zhou, M. Hu, *J. Mater. Chem. A* **2018**, *6*, 18533; d) B. Wu, Y. Zhou, M. Hu, *J. Phys. Chem. Lett.* **2018**, *9*, 5704; e) Y. Gao, W. Ning, X. Zhang, Y. Liu, Y. Zhou, D. Tang, *Nano Energy* **2021**, *82*, 105747.